JOURNAL OF AIRCRAFT
Vol. 29, No. 4, July–Aug. 1992

Self-Induced Roll Oscillations of Low-Aspect-Ratio Rectangular Wings

Daniel Levin*
NASA Ames Research Center, Moffett Field, California 94035
and
Joseph Katz†
San Diego State University, San Diego, California 92182

Experimental investigation of small-aspect-ratio rectangular wings mounted on a free-to-roll sting balance indicated that self-induced roll oscillations are possible when the aspect ratio of such wings is less than 0.5. The oscillations are probably driven by the periodic changes in the location and strength of the side-edge vortices, as it has been shown for the "wing rock" of delta wings, where similar changes in the leading-edge vortex strength and position cause the roll oscillations. During the roll-oscillation cycle, the roll angle, normal force, and the side force were recorded and presented for three wings with aspect ratios of 0.25, 0.35, and 0.47. These data indicate that the lift loss during roll oscillations of rectangular wings is less than what was measured for similar delta wings. Also, the flowfield of such slender rectangular wings at high angles of attack is more complicated than the flowfield over slender delta wings, due to the additional leading-edge vortex.

Introduction

FLOW-INDUCED oscillations of slender configurations, usually at high angles of attack, have been known to exist and mostly were avoided by excluding this angle-of-attack range from the flight envelope. At these high angles of attack, however, leading-edge (LE) vortices orginating from highly swept, slender lifting surfaces are capable of generating much-needed high-lift coefficients. Therefore, in many situations it would be advantageous to operate within this high-angle-of-attack range if some unintended instabilities, such as the limit-cycle roll oscillation or "wing rock," could be avoided. As a first step in developing control devices that will eliminate the self-induced oscillations, an effort was made to study the aerodynamic phenomena driving the roll oscillations. Most of these wind-tunnel experiments[1-6] concentrated on simple wing geometries, such as the delta wing, and measured various parameters, such as frequency, amplitude, and aerodynamic loads. Based on these experimental observations, mathematical models[7-14] of various complexity were developed to predict the envelope of self-induced roll oscillations, mainly in terms of leading-edge-sweep angle and the angle of attack.

Because wing rock is most likely to influence the high-angle-of-attack performance of a landing slender supersonic airplane, or a sharply maneuvering missile or fighter airplane with highly swept back strakes, most previous studies focused on such wing shapes (e.g., on delta wings). As a result, the leading-edge-sweep angle and the angle of attack were considered to be the dominant parameters in defining the envelope of self-induced roll oscillations (and even some maximum wing-sweep angles were quoted for possible limit-cycle oscillations).

In the present study it is demonstrated that the self-induced oscillations can be initiated by the interaction between concentrated vortices and a lifting surface that does not have a delta shape. In cases where the leading or side-edge vortex length is larger than the wing span, such instabilities can develop and if the wing damping is insufficient a limit-cycle roll oscillation will develop. For example, trailing-edge vortices of a canard[3] can induce roll instabilities on a wing placed downstream. Similarly, the side-edge vortices of a rectangular wing can induce roll oscillations when the wing aspect ratio becomes sufficiently small.

Consequently, for this experiment, several low-aspect-ratio, rectangular wings were examined in a free-to-roll test. It was found with this particular experimental setup that rectangular wings having an aspect ratio (AR) of less than 0.5 did exhibit continuous, limit-cycle, self-induced roll oscillations. These rectangular wing shapes were previously considered to be insensitive to limit-cycle oscillations, but based on the results of this study, it seems that for these self-induced oscillations of a lifting surface, wing aspect ratio is the dominant parameter and not leading-edge sweep.

Experimental Setup

The one-degree-of-freedom wing-rock experiment is described schematically in Fig. 1. The wing was mounted on a sting support in a free-to-roll manner by two low-friction bearings located inside the central cylinder (bearing friction was on the order of 0.002 N-cm). The aerodynamic loads were measured by a six-component balance located inside the central cylinder, behind the bearings. The balance was attached to the sting support and did not rotate with the wing. During the experiment the normal, axial, and side forces and the pitching and yawing moments were recorded in the sting balance frame of reference. The accuracy of the balance was better than ± 0.05 N for the force components and better than ± 0.3 N-cm for the moment components (in general, these values were less than 2% of the maximum loads during the experiment). Because the wing was free to roll, the rolling moment could not be measured directly, but the roll angle ϕ was recorded by a potentiometer located inside the cylinder ahead of the balance (see Fig. 1). Because wing roll damping increases with aspect-ratio, four flat-plate wings with aspect ratios of AR = 0.25, 0.35, 0.47, and 0.63 were fabricated for this test, but only the first three (shown in Fig. 2) would exhibit self-induced roll oscillations. Therefore, experimental data on the fourth wing is not presented. Based on the "wing rock"

Presented as Paper 90-2811 at the AIAA Atmospheric Flight Mechanics Conference, Aug. 20–22, 1990, Portland, OR; received Sept. 17, 1990; revision received May 8, 1991; accepted for publication May 27, 1991. Copyright © 1991 by the American Institute of Aeronautics and Astronautics, Inc. All rights reserved.

*Senior NRC Research Associate. Member AIAA.
†Professor, Department of Aerospace Engineering. Associate Fellow AIAA.

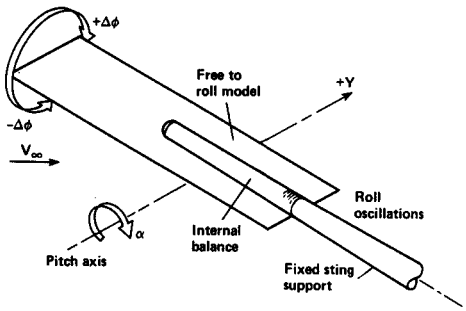

Fig. 1 Schematic description of the free-to-roll experiment.

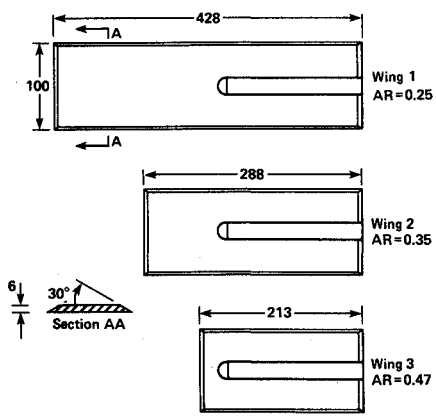

Fig. 2 Dimensions (in mm) of the three wing models.

characteristics of these four wings, we can conclude that rectangular wings with aspect ratios of AR > 0.5 are unlikely to undergo self-induced limit-cycle roll oscillation.

The open return wind tunnel used for this test has an inlet contraction ratio of 1:25 and test-section dimensions of 1 × 1 m. Test speeds varied between 10–20 m/s, corresponding to $Re_c \approx 0.15 \times 10^6$ to 0.57×10^6, where the Reynolds number is based on the corresponding wing chord. Because the leading edges of the models shown in Fig. 2 were sharp, it is believed that the effect of Reynolds number is relatively small and, therefore, the results of this small-scale testing are relevant to larger flight speeds and wing planforms.

Static Measurements

Prior to the free-to-roll tests, the static aerodynamic loads vs angle of attack were measured for the three rectangular wings. For these tests, the bearings were locked so that the wing was rigidly mounted to the internal balance. As an example, the normal-force coefficient C_N vs angle of attack α for the three wings is presented in Fig. 3. Each symbol on the figure represents the average value of 200 individual load readings of the six-component balance. For comparison, the "linear" normal-force coefficient slopes are presented for the low-angle-of-attack range. These curves represent the normal force due to attached flow on the wing and were obtained by a vortex-lattice method,[15] using a 6 × 6 grid per semispan. When comparing the experimental values of the normal force with the potential flow results, it becomes evident that the lift of small-aspect-ratio rectangluar wings is considerably larger[16] than predicted by linear theory. This is a result of the strong side-edge vortices, which are shown schematically in Fig. 4. Reference 16 also presented results for the effect of side edge vortex lift, which accounts for most of the lift of the small aspect ratio rectangular wing. In this particular case, the wing leading edge was sharp (see Fig. 2) and a bubble-shaped separated-flow region was visible (by smoke flow visualization) near the leading edge for angles of attack larger than 15 deg. Closer observation of this leading-edge separation indicated that it bears some similarity to the mushroom

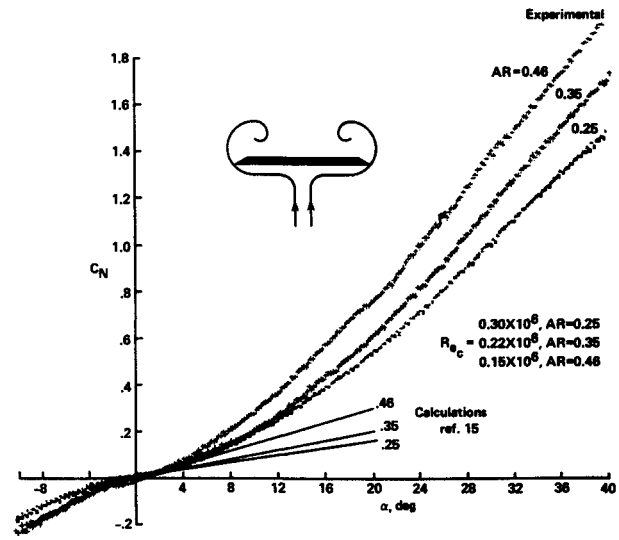

Fig. 3 Measured normal force (static) vs angle of attack for the three rectangular wings ("linear lift" indicate results obtained by potential-flow methods[15]).

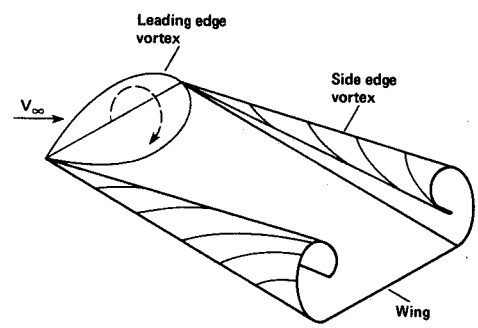

Fig. 4 Schematic description of the leading- and side-edge vortices, as were observed during flow visualizations (using both smoke and helium/soap bubble seeding).

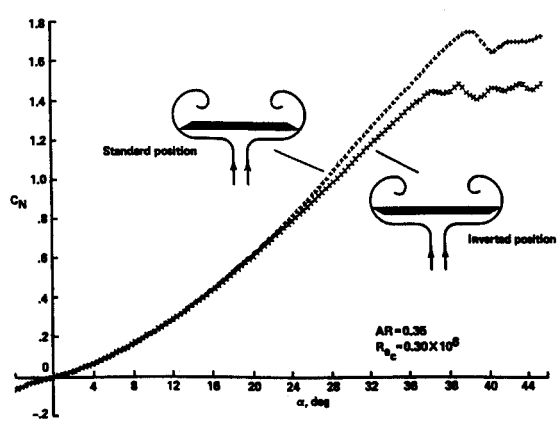

Fig. 5 Effect of leading-edge shape on the normal force of a slender rectangular wing (AR = 0.35).

shape observed[17] by surface-oil flow visualizations on larger-aspect-ratio rectangular wings. Figure 4 shows the average shape of this leading-edge bubble but periodic wake shedding, similar to the case of two-dimensional leading-edge separation[18] was present.

The leading-edge shape has been known to affect leading-edge (or side-edge) separated vortex strength[16] and vortex strength, usually, influences the aerodynamic loads. The order of magnitude of this effect is depicted by Fig. 5, which compares the normal-force coefficient obtained for wing 2 (AR = 0.35) in its standard position (see Sec. AA, in Fig. 2) and in its inverted position. This trend is very similar to the results obtained with inverted low-aspect-ratio rectangular wings[16] and delta wings[19] having the same leading-edge ge-

ometry. It is interesting to point out that the stronger side-edge vortex in the "standard position" case results in a delay in the wing stall (or vortex burst) and this wing generates more lift (or C_N) throughout the whole range of α.

In conclusion, the side-edge vortices of slender rectangular wings have a strong effect on the aerodynamic coefficients. The normal force is considerably increased by these side-edge vortices in the same manner as observed with low-aspect-ratio delta wings.

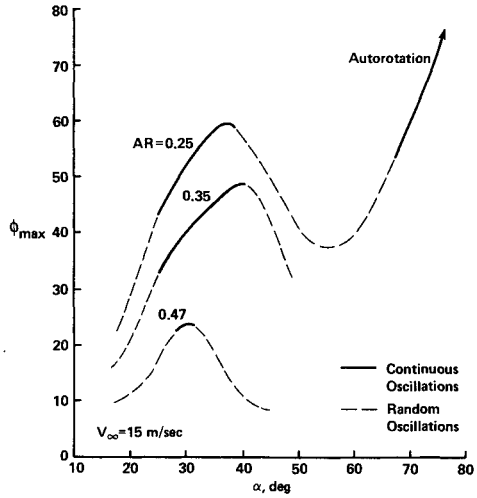

Fig. 6 Angle of attack and maximum roll angle range of the roll oscillations as observed during the present experiment (autorotation means that the wing continuously rotates in one of the directions).

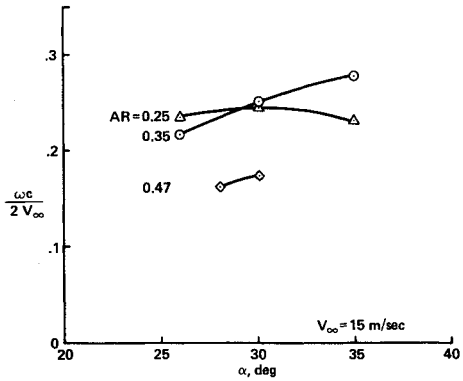

Fig. 7 Range of reduced frequencies observed during the present experiment.

Free-to-Roll Tests

For the dynamic tests, the model was mounted in the wind tunnel, as shown schematically in Fig. 1. During the test, the model's angle of attack was increased at a given airspeed V_∞ until a self-induced limit-cycle roll oscillation would develop (as indicated by the arrow in Fig. 1). Once the periodic oscillations developed, the angle of attack could be varied slightly within this "wing rock" range, which is shown in terms of angle of attack and maximum roll-angle amplitude for the three wings in Fig. 6. This range seemed not to depend on the direction of angle-of-attack sweep or on air speed, within the limited envelope of the experiment, and to depend mainly on angle of attack (this is an indication of lack of dependence on Reynolds number for the leading-edge and side-edge vortex lift). The wing with the highest aspect ratio of 0.47 had the narrowest range (27 deg $< \alpha <$ 30 deg) for continuous roll oscillations, as shown by the solid line in Fig. 6. The dashed lines indicate the maximum roll angle ϕ_{max} observed for this wing during random oscillations, which did not develop into steady periodic oscillations. These oscillations were random in their occurrence and not chaotic, moreover the frequency of their damped oscillations was close to the range presented in Fig. 7. As the wing aspect ratio becomes smaller, roll damping is reduced, and angle-of-attack range of self-induced oscillation increases. For wing No. 1 (AR = 0.25) the roll-angle amplitudes rapidly increased and at angles of attack of over 50 deg, the oscillations often turned into a steady spinning in one direction (autorotation).

The reduced frequency of the observed oscillations is shown in Fig. 7 and its magnitude is similar to values presented for delta wings in "wing rock" experiments.[2] As the wing aspect ratio was reduced from 0.47 to 0.37, the oscillation frequency increased. However, for the smallest-aspect-ratio wing, no additional increase in the reduced frequency was observed. It seemed that near the maximum roll-angle amplitude for this case (Φ_{max} is over 50 deg in Fig. 6) the motion was somewhat delayed and this caused the lower (than expected) oscillation range for this wing.

Typical dynamic results for the roll angle and side and normal force, as a function of time, are presented for the wing with AR = 0.35 in Figs. 8–10 (for three angles of attack). The roll angle data have a smooth sinusoidal shape whereas the aerodynamic-load data are less smooth. The symbols in

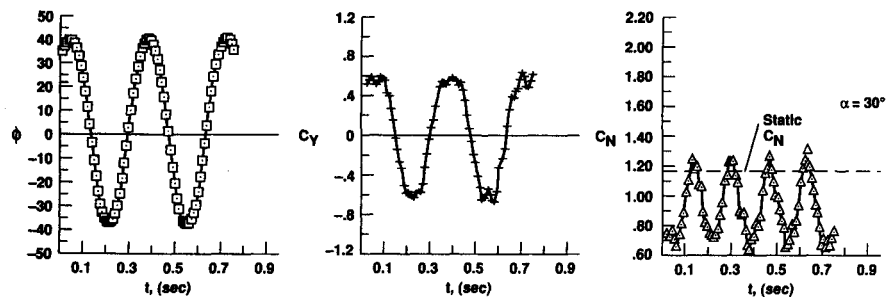

Fig. 8 Roll-angle, side-force, and normal-force variation during the wing rock cycle (AR = 0.35, α = 30 deg).

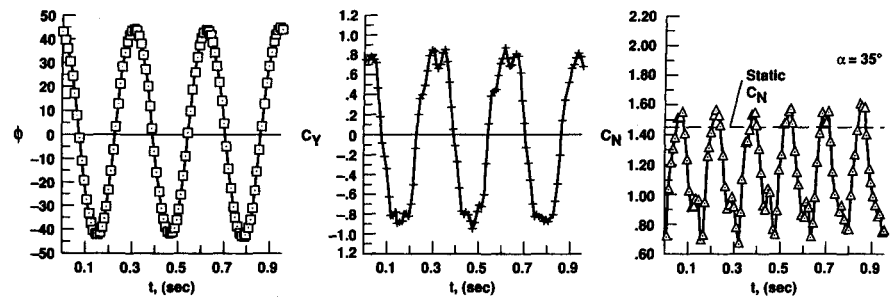

Fig. 9 Roll-angle, side-force, and normal-force variation during the wing rock cycle (AR = 0.35, α = 35 deg).

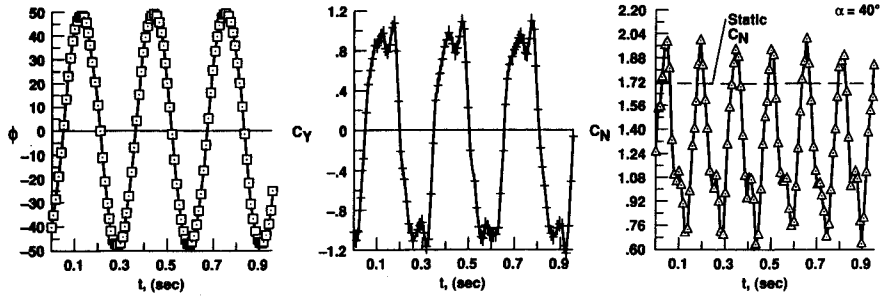

Fig. 10 Roll-angle, side-force, and normal-force variation during the wing rock cycle (AR = 0.35, α = 40 deg).

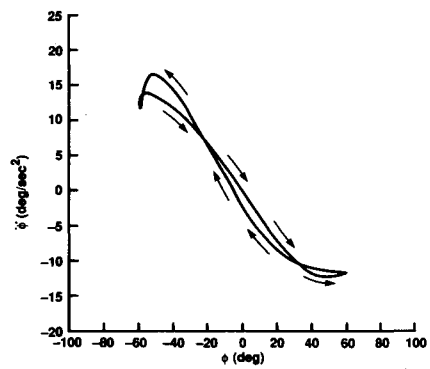

Fig. 11 Typical hysteresis loop of the rolling moment during the wing rock cycle.

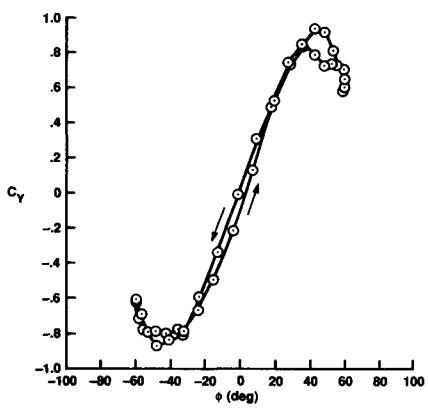

Fig. 12 Typical side-force-coefficient hysteresis loop during the wing rock cycle.

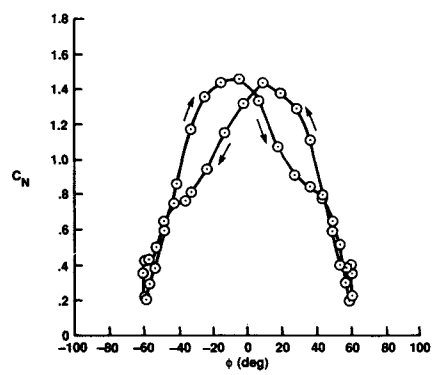

Fig. 13 Typical normal-force-coefficient hysteresis loop during the wing rock cycle.

the load data represent the measured value of the load and they are connected by straight line segments that indicate the sequence of the data (hence, cannot be considered as a curve fit for the data). The side force in general follows the pattern of the roll angle and near the maximum amplitudes the curve is less smooth, which is an indication of possible hysteresis there. The normal force oscillates at twice the frequency of the roll oscillations because the rolling motion either from left to right or from right to left will result in a complete normal-force cycle. So when the wing rotates from $-\phi_{max}$ to $+\phi_{max}$, one complete cycle of the normal force and only one-half of the roll-oscillation cycle has been completed. Also, the average dynamic normal force in Figs. 8–10 is less than the corresponding static force. This is mainly a result of the force normal to the wing being multiplied by $\cos\phi$ and also due to a larger average distance between the wing and the side-edge vortices in the dynamic case (when compared with the static data).

To investigate the phase relation between the roll angle ϕ and the aerodynamic loads, the hysteresis loops of Figs. 11–13 are presented. Here, for briefness, only the data for wing 2 (AR = 0.35) at α = 35 deg are provided, but these data are representative of the other wings.

The normal-force and side-force hysteresis loops clearly indicate that both clockwise and counterclockwise loops exists in the aerodynamic loads. The direction of the roll angle variation is depicted by the small arrows and it seems that there is a change in the direction of the hysteresis loops near the maximum roll angle amplitude range. In order to identify clearly the roll angle range where the oscillations are damped or driven, the rolling-moment hysteresis loop of Fig. 11 was indirectly constructed. The one degree-of-freedom equation of motion for the free-to-roll wing can be presented as

$$I_{xx}\ddot{\phi} = (\tfrac{1}{2}\rho V_\infty^2 Sb)C_l$$

where I_{xx} is the wing inertia, ρ is the air density, and S and b are the wing area and span, respectively. Once the roll angle $\phi(t)$, as presented in Figs. 8–10, is differentiated twice (numerically) the rolling moment C_l can be calculated from this equation and a hysteresis loop, such as those presented in Fig. 11, can be constructed. (Note that here C_l includes in addition to the aerodynamic moments, the damping due to the bearing friction.) Now, if we consider a positive rolling angle and moment, as indicated in Fig. 1, then a clockwise loop in the hysteresis loop represent an area where work is added to the system (the oscillations are being driven). Figure 11 indicates that this condition exists near the wing level position (when ϕ is close to zero). Similarly a counterclockwise loop indicates that work is consumed by the system and the motion is being damped (near the maximum roll angle region).

Discussion

Flow visualizations with helium/soap bubbles, laser sheet, and smoke revealed that the vortex structure shown schematically in Fig. 4 also existed during the dynamic tests. The large leading-edge separation bubble would pulsate with time, but this frequency was much larger (by more than one order of magnitude) than the "wing rock frequency." Also, the two side-edge vortices were visible and they oscillated up and down (relative to the wing) with the same frequency, but with a phase shift, in a manner similar to what is described in the literature for delta wings (for more information about the dynamic wake position on delta wings see, for example, Ref.

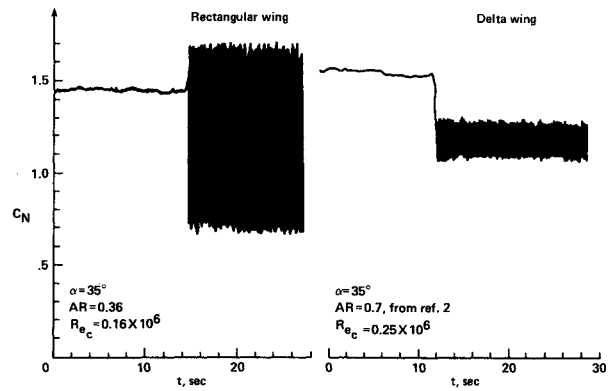

Fig. 14 Comparison of the normal-force coefficients during wing rock and steady-state conditions for rectangular and delta wings.

6). Side-edge vortex burst was visible at angles-of-attack of over 35 deg, but a careful documentation of the vortex-burst position with the current experimental setup was not attempted (because the helium/soap bubble probe-size affected the burst position).

The driving force of the "wing rock" oscillations, as most researchers[1-12] agree, is the dynamic vortex interaction and the associated flow lag effects caused by the motion of both the wing and the leading-edge vortices (or side-edge vortices in the present case). This flow lag affects both vortex strength and vortex position and, at least, the delay in the side-edge vortex motion relative to the wing is easily detected by flow visualization. It seems that during the oscillation cycle the vortex system above the up-moving semiwing moves closer to the surface, compared to the position of the vortex on the opposite semiwing. Consequently, a rolling moment in the direction of the rotation is generated near the wing leveled condition and, thereby, providing the energy to drive the motion.

So, in conclusion, it seems that the two strong longitudinal vortices drive the self-induced oscillations in cases of both the slender delta and the rectangular wings. There are some differences though in the aerodynamic behavior and, for example, the autorotation of the AR = 0.25 wing at high angles of attack has not been observed so far with delta wings. Also the change in the normal force due to the vortex motion is somewhat different for the two planforms. For the purpose of this comparison, Fig. 14 describes the measured steady state and the dynamic values of the normal force for the delta wing of Ref. 2 and for the present rectangular wing, No. 2. The normal force of a delta wing drops considerably during the roll oscillations, whereas the dynamic normal force of the rectangular wing reaches values (during the wing rock cycle) larger than the steady-state value. The larger amplitude of the oscillations in the case of the rectangular wing are due to the larger roll angles, but the difference in the average value of the lift cannot be explained easily. Possible future work should, therefore, concentrate on studying dynamic vortex strength, core locations, and effects of the motion on the vortex burst.

Conclusions

Vortex-induced lateral instabilities are not restricted to highly swept, slender wings and may appear in cases where the distance between a concentrated vortex and a lifting surface varies due to vehicle's motion. In the present study, the vortices originated from the side edges of the rectangular wings and the aerodynamic damping was altered by testing wings with different aspect ratios. When the aspect ratio was less than 0.5, the damping was low enough to allow the vortex-induced instabilities to develop into limit-cycle, continuous roll oscillations. It seems obvious that a possible control of the unintended wing rock can be based on manipulating the strength and location of the vortices that initially caused the motion.

At the higher angles of attack, in the case of the wing with aspect ratio of 0.25, the lateral instabilities led to a continuous autorotation resembling the tumbling motion of high-aspect-ratios wings. Also, the loss of the average lift during the roll oscillations was found to be less than the lift loss of similar slender delta wings.

Acknowledgment

This work was supported by NASA Ames Research Center, under Grant NCC-2-458, with James Ross as project monitor.

References

[1]Nguyen, L. T., Yip, L., and Chambers, J. R., "Self-Induced Wing Rock of Slender Delta Wings," AIAA Paper 81-1883, Seattle, WA, Aug. 1981.

[2]Levin, D., and Katz, J., "Dynamic Load Measurements with Delta Wings Undergoing Self-Induced Roll Oscillations," *Journal of Aircraft*, Vol. 21, No. 1, 1984, pp. 30–36.

[3]Katz, J., and Levin, D., "Self-Induced Roll-Oscillations Measured on a Delta Wing/Canard Configuration," *Journal of Aircraft*, Vol. 23, No. 11, 1986, pp. 801, 807.

[4]Jun, Y. W., and Nelson, R. C., "Leading Edge Vortex Dynamics on a Slender Oscillating Wing," *Journal of Aircraft*, Vol. 25, No. 9, 1988, pp. 815–819.

[5]Ng, T. T., Malcolm, G. N., and Lewis, L. C., "Flow Visualization Study of Delta Wing in Wing-Rock Motion," AIAA Paper 89-2187, Boston, MA, Aug. 1989.

[6]Arena, A. S., and Nelson, R. C., "The Effect of Asymmetric Vortex Wake Characteristics on a Slender Delta Wing Undergoing Wing Rock Motion," AIAA Paper 89-3348, Boston, MA, Aug. 1989.

[7]Konstadinopoulos, P., Mook, D. T., and Nayfeh, A. H., "Numerical Simulation of the Subsonic Wing Rock Phenomenon," AIAA Paper 83-2115, Gatlinburg, TN, Aug. 1983.

[8]Konstadinopoulos, P., Mook, D. T., and Nayfeh, A. H., "Subsonic Wing Rock of Slender Delta Wings," *Journal of Aircraft*, Vol. 22, No. 3, 1985, pp. 223–228.

[9]Ericsson, L. E., "The Fluid Mechanics of Slender Wing Rock," *Journal of Aircraft*, Vol. 21, No. 5, 1984, pp. 322–328.

[10]Ericsson, L. E., "Flow Phenomena Causing Wing and Body Rock," AIAA Paper 84-2177, Seattle, WA, Aug. 1984.

[11]Ericsson, L. E., "Analytic Prediction of the Maximum Amplitude of Slender Wing Rock," *Journal of Aircraft*, Vol. 26, No. 1, 1989, pp. 35–39.

[12]Hsu, C. H., and Lan, C. E., "Theory of Wing Rock," *Journal of Aircraft*, Vol. 22, No. 10, 1985, pp. 920–924.

[13]Elzebda, J. M., Mook, D. T., and Nayfeh, A. H., "Influence of Pitching Motion on Subsonic Wing Rock of Slender Delta Wings," *Journal of Aircraft*, Vol. 26, No. 6, 1989, pp. 503–508.

[14]Elzebda, J. M., Nayfeh, A. H., and Mook, D. T., "Development of an Analytical Model of Wing Rock for Slender Delta Wings," *Journal of Aircraft*, Vol. 26, No. 8, 1989, pp. 737–743.

[15]Katz, J., "Calculation of the Aerodynamic Forces on Automotive Lifting Surfaces," *Journal of Fluids Engineering*, Vol. 107, No. 4, 1985, pp. 438–443.

[16]Lamar, J. E., "Extension of Leading-Edge-Suction Analogy to Wings with Separated Flow Around the Side Edges at Subsonic Speeds," NASA TR R-428, Oct. 1974.

[17]Winkelmann, A. E., and Barlow, J. B., "Flowfield Model for a Rectangular Planform Wing Beyond Stall," *AIAA Journal*, Vol. 18, No. 8, 1980, pp. 1006–1008.

[18]McAlister, K. W., and Carr, L. W., "Water-Tunnel Experiments on an Oscillating Airfoil at *Re* = 21000," NASA TM 78446, March 1978.

[19]Katz, J., and Levin, D., "Measurements of Ground Effect for Delta Wings," *Journal of Aircraft*, Vol. 21, No. 6, 1984, pp. 441–443.